Measurement of the top quark mass at CDF using the "neutrino ϕ weighting" template method on a lepton plus isolated track sample

T. Aaltonen,[24] J. Adelman,[14] T. Akimoto,[56] B. Álvarez González[s],[12] S. Amerio[y],[44] D. Amidei,[35] A. Anastassov,[39] A. Annovi,[20] J. Antos,[15] G. Apollinari,[18] A. Apresyan,[49] T. Arisawa,[58] A. Artikov,[16] W. Ashmanskas,[18] A. Attal,[4] A. Aurisano,[54] F. Azfar,[43] P. Azzurri[z],[47] W. Badgett,[18] A. Barbaro-Galtieri,[29] V.E. Barnes,[49] B.A. Barnett,[26] V. Bartsch,[31] G. Bauer,[33] P.-H. Beauchemin,[34] F. Bedeschi,[47] D. Beecher,[31] S. Behari,[26] G. Bellettini[z],[47] J. Bellinger,[60] D. Benjamin,[17] A. Beretvas,[18] J. Beringer,[29] A. Bhatti,[51] M. Binkley,[18] D. Bisello[y],[44] I. Bizjak[ee],[31] R.E. Blair,[2] C. Blocker,[7] B. Blumenfeld,[26] A. Bocci,[17] A. Bodek,[50] V. Boisvert,[50] G. Bolla,[49] D. Bortoletto,[49] J. Boudreau,[48] A. Boveia,[11] B. Brau[a],[11] A. Bridgeman,[25] L. Brigliadori,[44] C. Bromberg,[36] E. Brubaker,[14] J. Budagov,[16] H.S. Budd,[50] S. Budd,[25] S. Burke,[18] K. Burkett,[18] G. Busetto[y],[44] P. Bussey,[22] A. Buzatu,[34] K. L. Byrum,[2] S. Cabrera[u],[17] C. Calancha,[32] M. Campanelli,[36] M. Campbell,[35] F. Canelli[14],[18] A. Canepa,[46] B. Carls,[25] D. Carlsmith,[60] R. Carosi,[47] S. Carrillo[n],[19] S. Carron,[34] B. Casal,[12] M. Casarsa,[18] A. Castro[x],[6] P. Catastini[aa],[47] D. Cauz[dd],[55] V. Cavaliere[aa],[47] M. Cavalli-Sforza,[4] A. Cerri,[29] L. Cerrito[o],[31] S.H. Chang,[28] Y.C. Chen,[1] M. Chertok,[8] G. Chiarelli,[47] G. Chlachidze,[18] F. Chlebana,[18] K. Cho,[28] D. Chokheli,[16] J.P. Chou,[23] G. Choudalakis,[33] S.H. Chuang,[53] K. Chung,[13] W.H. Chung,[60] Y.S. Chung,[50] T. Chwalek,[27] C.I. Ciobanu,[45] M.A. Ciocci[aa],[47] A. Clark,[21] D. Clark,[7] G. Compostella,[44] M.E. Convery,[18] J. Conway,[8] M. Cordelli,[20] G. Cortiana[y],[44] C.A. Cox,[8] D.J. Cox,[8] F. Crescioli[z],[47] C. Cuenca Almenar[u],[8] J. Cuevas[s],[12] R. Culbertson,[18] J.C. Cully,[35] D. Dagenhart,[18] M. Datta,[18] T. Davies,[22] P. de Barbaro,[50] S. De Cecco,[52] A. Deisher,[29] G. De Lorenzo,[4] M. Dell'Orso[z],[47] C. Deluca,[4] L. Demortier,[51] J. Deng,[17] M. Deninno,[6] P.F. Derwent,[18] G.P. di Giovanni,[45] C. Dionisi[cc],[52] B. Di Ruzza[dd],[55] J.R. Dittmann,[5] M. D'Onofrio,[4] S. Donati[z],[47] P. Dong,[9] J. Donini,[44] T. Dorigo,[44] S. Dube,[53] J. Efron,[40] A. Elagin,[54] R. Erbacher,[8] D. Errede,[25] S. Errede,[25] R. Eusebi,[18] H.C. Fang,[29] S. Farrington,[43] W.T. Fedorko,[14] R.G. Feild,[61] M. Feindt,[27] J.P. Fernandez,[32] C. Ferrazza[bb],[47] R. Field,[19] G. Flanagan,[49] R. Forrest,[8] M.J. Frank,[5] M. Franklin,[23] J.C. Freeman,[18] I. Furic,[19] M. Gallinaro,[52] J. Galyardt,[13] F. Garberson,[11] J.E. Garcia,[21] A.F. Garfinkel,[49] K. Genser,[18] H. Gerberich,[25] D. Gerdes,[35] A. Gessler,[27] S. Giagu[cc],[52] V. Giakoumopoulou,[3] P. Giannetti,[47] K. Gibson,[48] J.L. Gimmell,[50] C.M. Ginsburg,[18] N. Giokaris,[3] M. Giordani[dd],[55] P. Giromini,[20] M. Giunta[z],[47] G. Giurgiu,[26] V. Glagolev,[16] D. Glenzinski,[18] M. Gold,[38] N. Goldschmidt,[19] A. Golossanov,[18] G. Gomez,[12] G. Gomez-Ceballos,[33] M. Goncharov,[33] O. González,[32] I. Gorelov,[38] A.T. Goshaw,[17] K. Goulianos,[51] A. Gresele[y],[44] S. Grinstein,[23] C. Grosso-Pilcher,[14] R.C. Group,[18] U. Grundler,[25] J. Guimaraes da Costa,[23] Z. Gunay-Unalan,[36] C. Haber,[29] K. Hahn,[33] S.R. Hahn,[18] E. Halkiadakis,[53] B.-Y. Han,[50] J.Y. Han,[50] F. Happacher,[20] K. Hara,[56] D. Hare,[53] M. Hare,[57] S. Harper,[43] R.F. Harr,[59] R.M. Harris,[18] M. Hartz,[48] K. Hatakeyama,[51] C. Hays,[43] M. Heck,[27] A. Heijboer,[46] J. Heinrich,[46] C. Henderson,[33] M. Herndon,[60] J. Heuser,[27] S. Hewamanage,[5] D. Hidas,[17] C.S. Hill[c],[11] D. Hirschbuehl,[27] A. Hocker,[18] S. Hou,[1] M. Houlden,[30] S.-C. Hsu,[29] B.T. Huffman,[43] R.E. Hughes,[40] U. Husemann,[61] M. Hussein,[36] J. Huston,[36] J. Incandela,[11] G. Introzzi,[47] M. Iori[cc],[52] A. Ivanov,[8] E. James,[18] D. Jang,[13] B. Jayatilaka,[17] E.J. Jeon,[28] M.K. Jha,[6] S. Jindariani,[18] W. Johnson,[8] M. Jones,[49] K.K. Joo,[28] S.Y. Jun,[13] J.E. Jung,[28] T.R. Junk,[18] T. Kamon,[54] D. Kar,[19] P.E. Karchin,[59] Y. Kato[l],[42] R. Kephart,[18] J. Keung,[46] V. Khotilovich,[54] B. Kilminster,[18] D.H. Kim,[28] H.S. Kim,[28] H.W. Kim,[28] J.E. Kim,[28] M.J. Kim,[20] S.B. Kim,[28] S.H. Kim,[56] Y.K. Kim,[14] N. Kimura,[56] L. Kirsch,[7] S. Klimenko,[19] B. Knuteson,[33] B.R. Ko,[17] K. Kondo,[58] D.J. Kong,[28] J. Konigsberg,[19] A. Korytov,[19] A.V. Kotwal,[17] M. Kreps,[27] J. Kroll,[46] D. Krop,[14] N. Krumnack,[5] M. Kruse,[17] V. Krutelyov,[11] T. Kubo,[56] T. Kuhr,[27] N.P. Kulkarni,[59] M. Kurata,[56] S. Kwang,[14] A.T. Laasanen,[49] S. Lami,[47] S. Lammel,[18] M. Lancaster,[31] R.L. Lander,[8] K. Lannon[r],[40] A. Lath,[53] G. Latino[aa],[47] I. Lazzizzera[y],[44] T. LeCompte,[2] E. Lee,[54] H.S. Lee,[14] S.W. Lee[t],[54] S. Leone,[47] J.D. Lewis,[18] C.-S. Lin,[29] J. Linacre,[43] M. Lindgren,[18] E. Lipeles,[46] A. Lister,[8] D.O. Litvintsev,[18] C. Liu,[48] T. Liu,[18] N.S. Lockyer,[46] A. Loginov,[61] M. Loreti[y],[44] L. Lovas,[15] D. Lucchesi[y],[44] C. Luci[cc],[52] J. Lueck,[27] P. Lujan,[29] P. Lukens,[18] G. Lungu,[51] L. Lyons,[43] J. Lys,[29] R. Lysak,[15] D. MacQueen,[34] R. Madrak,[18] K. Maeshima,[18] K. Makhoul,[33] T. Maki,[24] P. Maksimovic,[26] S. Malde,[43] S. Malik,[31] G. Manca[e],[30] A. Manousakis-Katsikakis,[3] F. Margaroli,[49] C. Marino,[27] C.P. Marino,[25] A. Martin,[61] V. Martin[k],[22] M. Martínez,[4] R. Martínez-Ballarín,[32] T. Maruyama,[56] P. Mastrandrea,[52] T. Masubuchi,[56] M. Mathis,[26] M.E. Mattson,[59] P. Mazzanti,[6] K.S. McFarland,[50] P. McIntyre,[54] R. McNulty[j],[30] A. Mehta,[30] P. Mehtala,[24] A. Menzione,[47] P. Merkel,[49] C. Mesropian,[51] T. Miao,[18] N. Miladinovic,[7] R. Miller,[36] C. Mills,[23] M. Milnik,[27] A. Mitra,[1] G. Mitselmakher,[19] H. Miyake,[56] N. Moggi,[6] C.S. Moon,[28] R. Moore,[18] M.J. Morello[z],[47] J. Morlock,[27] P. Movilla Fernandez,[18] J. Mülmenstädt,[29] A. Mukherjee,[18] Th. Muller,[27] R. Mumford,[26] P. Murat,[18] M. Mussini[x],[6] J. Nachtman,[18] Y. Nagai,[56] A. Nagano,[56] J. Naganoma,[56] K. Nakamura,[56] I. Nakano,[41] A. Napier,[57]

V. Necula,[17] J. Nett,[60] C. Neu[v],[46] M.S. Neubauer,[25] S. Neubauer,[27] J. Nielsen[g],[29] L. Nodulman,[2] M. Norman,[10] O. Norniella,[25] E. Nurse,[31] L. Oakes,[43] S.H. Oh,[17] Y.D. Oh,[28] I. Oksuzian,[19] T. Okusawa,[42] R. Orava,[24] K. Osterberg,[24] S. Pagan Griso[y],[44] E. Palencia,[18] V. Papadimitriou,[18] A. Papaikonomou,[27] A.A. Paramonov,[14] B. Parks,[40] S. Pashapour,[34] J. Patrick,[18] G. Pauletta[dd],[55] M. Paulini,[13] C. Paus,[33] T. Peiffer,[27] D.E. Pellett,[8] A. Penzo,[55] T.J. Phillips,[17] G. Piacentino,[47] E. Pianori,[46] L. Pinera,[19] K. Pitts,[25] C. Plager,[9] L. Pondrom,[60] O. Poukhov*,[16] N. Pounder,[43] F. Prakoshyn,[16] A. Pronko,[18] J. Proudfoot,[2] F. Ptohos[i],[18] E. Pueschel,[13] G. Punzi[z],[47] J. Pursley,[60] J. Rademacker[c],[43] A. Rahaman,[48] V. Ramakrishnan,[60] N. Ranjan,[49] I. Redondo,[32] P. Renton,[43] M. Renz,[27] M. Rescigno,[52] S. Richter,[27] F. Rimondi[x],[6] L. Ristori,[47] A. Robson,[22] T. Rodrigo,[12] T. Rodriguez,[46] E. Rogers,[25] S. Rolli,[57] R. Roser,[18] M. Rossi,[55] R. Rossin,[11] P. Roy,[34] A. Ruiz,[12] J. Russ,[13] V. Rusu,[18] B. Rutherford,[18] H. Saarikko,[24] A. Safonov,[54] W.K. Sakumoto,[50] O. Saltó,[4] L. Santi[dd],[55] S. Sarkar[cc],[52] L. Sartori,[47] K. Sato,[18] A. Savoy-Navarro,[45] P. Schlabach,[18] A. Schmidt,[27] E.E. Schmidt,[18] M.A. Schmidt,[14] M.P. Schmidt*,[61] M. Schmitt,[39] T. Schwarz,[8] L. Scodellaro,[12] A. Scribano[aa],[47] F. Scuri,[47] A. Sedov,[49] S. Seidel,[38] Y. Seiya,[42] A. Semenov,[16] L. Sexton-Kennedy,[18] F. Sforza,[47] A. Sfyrla,[25] S.Z. Shalhout,[59] T. Shears,[30] P.F. Shepard,[48] M. Shimojima[q],[56] S. Shiraishi,[14] M. Shochet,[14] Y. Shon,[60] I. Shreyber,[37] A. Sidoti,[47] P. Sinervo,[34] A. Sisakyan,[16] A.J. Slaughter,[18] J. Slaunwhite,[40] K. Sliwa,[57] J.R. Smith,[8] F.D. Snider,[18] R. Snihur,[34] A. Soha,[8] S. Somalwar,[53] V. Sorin,[36] J. Spalding,[18] T. Spreitzer,[34] P. Squillacioti[aa],[47] M. Stanitzki,[61] R. St. Denis,[22] B. Stelzer,[34] O. Stelzer-Chilton,[34] D. Stentz,[39] J. Strologas,[38] G.L. Strycker,[35] D. Stuart,[11] J.S. Suh,[28] A. Sukhanov,[19] I. Suslov,[16] T. Suzuki,[56] A. Taffard[f],[25] R. Takashima,[41] Y. Takeuchi,[56] R. Tanaka,[41] M. Tecchio,[35] P.K. Teng,[1] K. Terashi,[51] J. Thom[h],[18] A.S. Thompson,[22] G.A. Thompson,[25] E. Thomson,[46] P. Tipton,[61] P. Ttito-Guzmán,[32] S. Tkaczyk,[18] D. Toback,[54] S. Tokar,[15] K. Tollefson,[36] T. Tomura,[56] D. Tonelli,[18] S. Torre,[20] D. Torretta,[18] P. Totaro[dd],[55] S. Tourneur,[45] M. Trovato,[47] S.-Y. Tsai,[1] Y. Tu,[46] N. Turini[aa],[47] F. Ukegawa,[56] S. Vallecorsa,[21] N. van Remortel[b],[24] A. Varganov,[35] E. Vataga[bb],[47] F. Vázquez[n],[19] G. Velev,[18] C. Vellidis,[3] M. Vidal,[32] R. Vidal,[18] I. Vila,[12] R. Vilar,[12] T. Vine,[31] M. Vogel,[38] I. Volobouev[t],[29] G. Volpi[z],[47] P. Wagner,[46] R.G. Wagner,[2] R.L. Wagner,[18] W. Wagner[w],[27] J. Wagner-Kuhr,[27] T. Wakisaka,[42] R. Wallny,[9] S.M. Wang,[1] A. Warburton,[34] D. Waters,[31] M. Weinberger,[54] J. Weinelt,[27] W.C. Wester III,[18] B. Whitehouse,[57] D. Whiteson[f],[46] A.B. Wicklund,[2] E. Wicklund,[18] S. Wilbur,[14] G. Williams,[34] H.H. Williams,[46] P. Wilson,[18] B.L. Winer,[40] P. Wittich[h],[18] S. Wolbers,[18] C. Wolfe,[14] T. Wright,[35] X. Wu,[21] F. Würthwein,[10] S. Xie,[33] A. Yagil,[10] K. Yamamoto,[42] J. Yamaoka,[17] U.K. Yang[p],[14] Y.C. Yang,[28] W.M. Yao,[29] G.P. Yeh,[18] J. Yoh,[18] K. Yorita,[58] T. Yoshida[m],[42] G.B. Yu,[50] I. Yu,[28] S.S. Yu,[18] J.C. Yun,[18] L. Zanello[cc],[52] A. Zanetti,[55] X. Zhang,[25] Y. Zheng[d],[9] and S. Zucchelli[x],[6]

(CDF Collaboration†)

[1] *Institute of Physics, Academia Sinica, Taipei, Taiwan 11529, Republic of China*
[2] *Argonne National Laboratory, Argonne, Illinois 60439*
[3] *University of Athens, 157 71 Athens, Greece*
[4] *Institut de Fisica d'Altes Energies, Universitat Autonoma de Barcelona, E-08193, Bellaterra (Barcelona), Spain*
[5] *Baylor University, Waco, Texas 76798*
[6] *Istituto Nazionale di Fisica Nucleare Bologna, [x] University of Bologna, I-40127 Bologna, Italy*
[7] *Brandeis University, Waltham, Massachusetts 02254*
[8] *University of California, Davis, Davis, California 95616*
[9] *University of California, Los Angeles, Los Angeles, California 90024*
[10] *University of California, San Diego, La Jolla, California 92093*
[11] *University of California, Santa Barbara, Santa Barbara, California 93106*
[12] *Instituto de Fisica de Cantabria, CSIC-University of Cantabria, 39005 Santander, Spain*
[13] *Carnegie Mellon University, Pittsburgh, PA 15213*
[14] *Enrico Fermi Institute, University of Chicago, Chicago, Illinois 60637*
[15] *Comenius University, 842 48 Bratislava, Slovakia; Institute of Experimental Physics, 040 01 Kosice, Slovakia*
[16] *Joint Institute for Nuclear Research, RU-141980 Dubna, Russia*
[17] *Duke University, Durham, North Carolina 27708*
[18] *Fermi National Accelerator Laboratory, Batavia, Illinois 60510*
[19] *University of Florida, Gainesville, Florida 32611*
[20] *Laboratori Nazionali di Frascati, Istituto Nazionale di Fisica Nucleare, I-00044 Frascati, Italy*
[21] *University of Geneva, CH-1211 Geneva 4, Switzerland*
[22] *Glasgow University, Glasgow G12 8QQ, United Kingdom*
[23] *Harvard University, Cambridge, Massachusetts 02138*
[24] *Division of High Energy Physics, Department of Physics, University of Helsinki and Helsinki Institute of Physics, FIN-00014, Helsinki, Finland*
[25] *University of Illinois, Urbana, Illinois 61801*
[26] *The Johns Hopkins University, Baltimore, Maryland 21218*
[27] *Institut für Experimentelle Kernphysik, Universität Karlsruhe, 76128 Karlsruhe, Germany*

[28] Center for High Energy Physics: Kyungpook National University, Daegu 702-701, Korea; Seoul National University, Seoul 151-742, Korea; Sungkyunkwan University, Suwon 440-746, Korea; Korea Institute of Science and Technology Information, Daejeon, 305-806, Korea; Chonnam National University, Gwangju, 500-757, Korea
[29] Ernest Orlando Lawrence Berkeley National Laboratory, Berkeley, California 94720
[30] University of Liverpool, Liverpool L69 7ZE, United Kingdom
[31] University College London, London WC1E 6BT, United Kingdom
[32] Centro de Investigaciones Energeticas Medioambientales y Tecnologicas, E-28040 Madrid, Spain
[33] Massachusetts Institute of Technology, Cambridge, Massachusetts 02139
[34] Institute of Particle Physics: McGill University, Montréal, Québec, Canada H3A 2T8; Simon Fraser University, Burnaby, British Columbia, Canada V5A 1S6; University of Toronto, Toronto, Ontario, Canada M5S 1A7; and TRIUMF, Vancouver, British Columbia, Canada V6T 2A3
[35] University of Michigan, Ann Arbor, Michigan 48109
[36] Michigan State University, East Lansing, Michigan 48824
[37] Institution for Theoretical and Experimental Physics, ITEP, Moscow 117259, Russia
[38] University of New Mexico, Albuquerque, New Mexico 87131
[39] Northwestern University, Evanston, Illinois 60208
[40] The Ohio State University, Columbus, Ohio 43210
[41] Okayama University, Okayama 700-8530, Japan
[42] Osaka City University, Osaka 588, Japan
[43] University of Oxford, Oxford OX1 3RH, United Kingdom
[44] Istituto Nazionale di Fisica Nucleare, Sezione di Padova-Trento, [y] University of Padova, I-35131 Padova, Italy
[45] LPNHE, Universite Pierre et Marie Curie/IN2P3-CNRS, UMR7585, Paris, F-75252 France
[46] University of Pennsylvania, Philadelphia, Pennsylvania 19104
[47] Istituto Nazionale di Fisica Nucleare Pisa, [z] University of Pisa, [aa] University of Siena and [bb] Scuola Normale Superiore, I-56127 Pisa, Italy
[48] University of Pittsburgh, Pittsburgh, Pennsylvania 15260
[49] Purdue University, West Lafayette, Indiana 47907
[50] University of Rochester, Rochester, New York 14627
[51] The Rockefeller University, New York, New York 10021
[52] Istituto Nazionale di Fisica Nucleare, Sezione di Roma 1, [cc] Sapienza Università di Roma, I-00185 Roma, Italy
[53] Rutgers University, Piscataway, New Jersey 08855
[54] Texas A&M University, College Station, Texas 77843
[55] Istituto Nazionale di Fisica Nucleare Trieste/Udine, I-34100 Trieste, [dd] University of Trieste/Udine, I-33100 Udine, Italy
[56] University of Tsukuba, Tsukuba, Ibaraki 305, Japan
[57] Tufts University, Medford, Massachusetts 02155
[58] Waseda University, Tokyo 169, Japan
[59] Wayne State University, Detroit, Michigan 48201
[60] University of Wisconsin, Madison, Wisconsin 53706
[61] Yale University, New Haven, Connecticut 06520

We present a measurement of the top quark mass with $t\bar{t}$ dilepton events produced in $p\bar{p}$ collisions at the Fermilab Tevatron ($\sqrt{s}$=1.96 TeV) and collected by the CDF II detector. A sample of 328 events with a charged electron or muon and an isolated track, corresponding to an integrated luminosity of 2.9 fb^{-1}, are selected as $t\bar{t}$ candidates. To account for the unconstrained event kinematics, we scan over the phase space of the azimuthal angles $(\phi_{\nu_1}, \phi_{\nu_2})$ of neutrinos and reconstruct the top quark mass for each $\phi_{\nu_1}, \phi_{\nu_2}$ pair by minimizing a χ^2 function in the $t\bar{t}$ dilepton hypothesis. We assign χ^2-dependent weights to the solutions in order to build a preferred mass for each event. Preferred mass distributions (templates) are built from simulated $t\bar{t}$ and background events, and parameterized in order to provide continuous probability density functions. A likelihood fit to the mass distribution in data as a weighted sum of signal and background probability density functions gives a top quark mass of $165.5^{+3.4}_{-3.3}$(stat.)$\pm$3.1(syst.) GeV/c^2.

PACS numbers: 14.65.Ha, 13.85.Qk, 12.15.Ff

*Deceased

†With visitors from [a]University of Massachusetts Amherst,

I. INTRODUCTION

The standard model (SM) explains the non-zero weak boson masses by spontaneous breaking of the electroweak (EW) symmetry induced by the Higgs field [1]. Also, non-zero quark masses are generated by the coupling of the Higgs doublet with the fundamental fermions. However, their values are not predicted since they are proportional to the unknown Yukawa couplings of each quark. The enormous top quark mass, which has a value comparable to the EW scale, justifies the suspect that this quark may play a special role in the mechanism which breaks EW symmetry. In addition, because of its large mass, the top quark gives the largest contribution to loop corrections in the W propagator. Within the SM, the correlation between the top mass and the W mass induced by these corrections allows setting limits on the mass of the yet unobserved Higgs boson, and favor a relatively light Higgs. A more accurate measurement of the top quark mass will tighten the SM predicted region for the Higgs boson mass.

According to the SM, at the Tevatron's 1.96 TeV energy top quarks are dominantly produced in pairs, by $q\bar{q}$ annihilation in $\sim 85\%$ of the cases and by gluon fusion in the remaining $\sim 15\%$ [2]. Due to its extremely short lifetime, which in the SM is expected to be about 10^{-25} s, the top quark decays before hadronizing in $\sim 100\%$ of cases into a W boson and b-quark [3]. Subsequently the W boson can either decay into quarks as a $q\bar{q}'$ pair or into a charged lepton-neutrino pair. This allows classifying the $t\bar{t}$ candidate events into three final states: all-hadronic, lepton+jets, or dilepton, depending on the decay modes of the two W bosons in the event. The all-hadronic state, where both W's decay hadronically (about 46% of $t\bar{t}$ events), is characterized by six or more jets in the event. The lepton+jets final state contains one electron or muon (about 30% of $t\bar{t}$ events), four or more jets, and one neutrino. Analyses dealing with the lepton+jets final state have provided the most precise top quark mass measurements, due to an optimal compromise between statistics and backgrounds. The dilepton final state, which is defined by the presence of two leptons (electrons or muons, about 5% of $t\bar{t}$ events), two or more jets, and large missing transverse energy from the two neutrinos, is the cleanest one, but suffers from the poorest statistics.

It is important to perform measurements using independent data samples in all final states in order to improve the precision on the top quark mass and to be able to cross-check the results. Once the channel-specific SM backgrounds have been removed, discrepancies in the results across different samples could provide hints of new physics. The present analysis is performed in the dilepton final state by means of lepton+track ("LTRK") top-pair selection. This selection is chosen to collect a large portion of events (about 45%) not involved in the other CDF high precision top mass analyses performed in the dilepton final state [4, 5].

The paper reports a measurement of the top quark mass with data collected by CDF II before spring 2008, corresponding to 2.9 fb^{-1} of integrated luminosity. We select $t\bar{t}$ candidate events in dilepton channel by requiring a well identified electron or muon plus a second, more loosely defined lepton, which is an isolated track. The measurement of the top quark mass in this channel is particularly challenging because of the two neutrinos in the final state. The kinematics is under-constrained and therefore assumptions on some missing final state observables are needed in order to reconstruct the event. In order to constrain the kinematics, we scan over the space of possibilities for the azimuthal angles of the two neutrinos, and reconstruct the top quark mass by minimizing a χ^2 function using the $t\bar{t}$ dilepton hypothesis. A weighted average over a grid of the azimuthal neutrino angles $(\phi_{\nu_1}, \phi_{\nu_2})$ returns a single top quark mass value per event. In this analysis the Breit-Wigner probability distribution function with a top quark mass–dependent decay width is applied in the kinematical event reconstruction, which helps to decrease the statistical uncertainty by 20% compared to the method described in [6]. The top quark mass distribution in the data is fitted to the parameterized signal and background templates, and the mass is extracted as the one corresponding to the best fit.

Sections II and III describe the detector and the selection of the data sample. Section IV gives an overview of the method used to reconstruct the events and to derive a single value of the top quark mass for each event. Section V defines the parameterization of signal and background mass distributions and the likelihood function used to fit the data to these distributions. Section VI describes the studies performed to calibrate the method, sections VII and VIII present the results and the systematic uncer-

Amherst, Massachusetts 01003, [b]Universiteit Antwerpen, B-2610 Antwerp, Belgium, [c]University of Bristol, Bristol BS8 1TL, United Kingdom, [d]Chinese Academy of Sciences, Beijing 100864, China, [e]Istituto Nazionale di Fisica Nucleare, Sezione di Cagliari, 09042 Monserrato (Cagliari), Italy, [f]University of California Irvine, Irvine, CA 92697, [g]University of California Santa Cruz, Santa Cruz, CA 95064, [h]Cornell University, Ithaca, NY 14853, [i]University of Cyprus, Nicosia CY-1678, Cyprus, [j]University College Dublin, Dublin 4, Ireland, [k]University of Edinburgh, Edinburgh EH9 3JZ, United Kingdom, [l]University of Fukui, Fukui City, Fukui Prefecture, Japan 910-0017 [m]Kinki University, Higashi-Osaka City, Japan 577-8502 [n]Universidad Iberoamericana, Mexico D.F., Mexico, [o]Queen Mary, University of London, London, E1 4NS, England, [p]University of Manchester, Manchester M13 9PL, England, [q]Nagasaki Institute of Applied Science, Nagasaki, Japan, [r]University of Notre Dame, Notre Dame, IN 46556, [s]University de Oviedo, E-33007 Oviedo, Spain, [t]Texas Tech University, Lubbock, TX 79609, [u]IFIC(CSIC-Universitat de Valencia), 46071 Valencia, Spain, [v]University of Virginia, Charlottesville, VA 22904, [w]Bergische Universität Wuppertal, 42097 Wuppertal, Germany, [ee]On leave from J. Stefan Institute, Ljubljana, Slovenia,

tainties, and section IX gives the conclusions.

II. THE CDF II DETECTOR

The Collider Detector at Fermilab was upgraded in the year 2000 (CDF II, Figure 1) in order to be able to handle the higher collision rate from the increased Tevatron luminosity. CDF II is a cylindrically and forward-backward symmetric apparatus detecting the products of the $p\bar{p}$ collisions over almost the full solid angle. A cylindrical (r, ϕ, z) coordinate system is used to describe the detector geometry. The origin of the reference system is the geometric center of the detector, with the z axis pointing along the proton beam. The pseudorapidity η is defined by $\eta \equiv -\ln(\tan(\theta/2))$, where θ is the polar angle relative to the z axis. The detector elements which are most relevant for this analysis are described below. A more complete description of the detector can be found elsewhere [7].

The tracking system consists of an inner silicon system and an outer gas drift chamber, the Central Outer Tracker (COT). The entire tracker is enclosed in a superconducting solenoid which generates a nearly uniform 1.4 T magnetic field in the z direction and provides precision tracking and momentum measurement of charged particles within $|\eta| \leq 1$. The silicon tracker, which covers the $|\eta| < 2$ region, is composed of the innermost detector (L00) [8], the Silicon Vertex Detector (SVXII) [9], and the Intermediate Silicon Layers (ISL) [10]. L00 is a layer of single-sided radiation-hardened silicon strips mounted directly on the beam pipe at a radius ranging from 1.35 cm to 1.62 cm. SVXII is an approximately 95 cm long cylinder of five layers of double-sided silicon microstrips covering a radial region between 2.5 cm and 10.7 cm. The ISL employs the same sensors as SVXII and covers the radial region between 20 cm and 28 cm, with one layer in the central region and two layers at larger angles. The COT [11], which spans 310 cm in length at a radial distance ranging between 43 and 132 cm, contains four axial and four $\pm 2^\circ$ stereo superlayers of azimuthal drift cells. Axial and stereo superlayers alternate radially with one another. The COT provides full coverage in the $|\eta| \leq 1$ region, with reduced coverage in the region $1 < |\eta| \leq 2$.

Sampling calorimeters, divided into an inner electromagnetic and an outer hadronic compartment, surround the solenoid. Except for limited areas of non-instrumented regions ("cracks"), the calorimeters provide full azimuthal coverage within $|\eta| \leq 3.6$. All calorimeters are split into towers with projective geometry pointing at the nominal interaction vertex [7]. Embedded in the electromagnetic compartment, a shower maximum detector provides good position measurements of the electromagnetic showers and is used in electron identification [12].

The muon detection system consists of stacks of drift chamber modules backed by plastic scintillator counters. The stacks are four layer deep with laterally staggered cells from layer to layer to compensate for cell-edge inefficiencies. Four separate systems are used to detect muons in the $|\eta| < 1.5$ region. The central muon detector (CMU) [13] is located behind the central hadronic calorimeter at a radius of ~ 3.5 m from the beam axis, covering the $|\eta| < 0.63$ region. The central muon upgrade detector (CMP) is arranged to enclose the $|\eta| < 0.54$ region in an approximate four-sided box. It is separated from the CMU by the additional shielding provided by 60 cm of steel. The central muon extension (CMX) extends the muon identification to the region $0.6 < |\eta| < 1.0$. The more forward region ($1.0 < |\eta| < 1.5$) is covered by the intermediate muon detector (IMU). Table I summarizes the characteristics of the CDF sub-detectors used in this analysis.

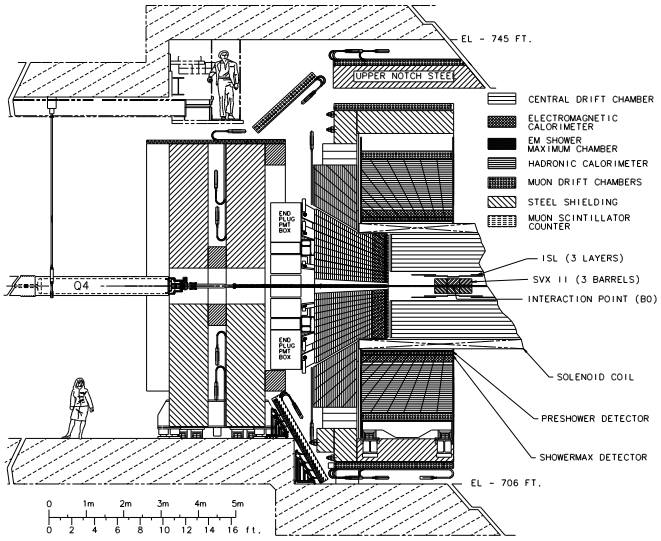

FIG. 1: Elevation view of half of the CDF II detector, showing the inner microstrip detector, the Central Outer Tracker drift chamber, the electromagnetic and hadronic calorimeters, the muon drift chambers and scintillation counters.

CDF uses a three-level trigger system to select events to be recorded on tape, filtering the interactions from a 1.7 MHz average bunch crossing rate to an output of 75-100 Hz. This analysis uses data from triggers based on leptons with high transverse momentum P_T, as expected from the leptonically decaying W's in the event. The first two trigger levels perform limited reconstruction using dedicated hardware, which reconstructs tracks from the COT in the $r-\phi$ plane with a transverse momentum resolution better than $2\% \times P_T^2$ [GeV/c] [18]. The electron trigger requires a coincidence of a COT track with an electromagnetic cluster in the central calorimeter, while the muon trigger requires that a COT track points toward a set of hits in the muon chambers. The third level is a software trigger which runs offline algorithms optimized for speed.

TABLE I: CDF II sub-detectors, purposes, resolutions or acceptances.

Component	Purpose	Resolution/Acceptance	Reference
Silicon System	Hit position	11 μm (L00)	[8]
		9 μm (SVXII)	[9]
		16÷23 μm (ISL)	[7]
	Impact parameter	40 μm	
	Interaction Vertex Position	70 μm	
COT	Hit position	140 μm	[11]
	Momentum measurement	$\frac{\sigma_{P_T}}{P_T} = 0.15 \times P_T[GeV/c]$	
Central Calorimeters			
Electro-magnetic calorimeter	Energy	$\frac{\sigma_E}{E} = 13.5\%/\sqrt{E_T[GeV]} \oplus 2\%$	[14]
Shower Max Detector	Position	2 mm	[15]
Hadron Calorimeter	Energy	$\frac{\sigma_E}{E} = 50.0\%/\sqrt{E[GeV]} \oplus 3\%$	[16]
Wall Hadron Calorimeter	Energy	$\frac{\sigma_E}{E} = 75.0\%/\sqrt{E[GeV]} \oplus 4\%$	[7]
Forward Calorimeters			
Electro-magnetic calorimeter	Energy	$\frac{\sigma_E}{E} = 16.0\%/\sqrt{E[GeV]} \oplus 1\%$	[17]
Shower Max Detector	Position	1 mm	[12]
Hadron Calorimeter	Energy	$\frac{\sigma_E}{E} = 80.0\%/\sqrt{E[GeV]} \oplus 5\%$	[7]
Muon Systems	Muon Detection		
CMU		P_T >1.4 GeV/c	[13],[7]
CMP		P_T >2.2 GeV/c	[7]
CMX		P_T >1.4 GeV/c	[7]

III. DATA SAMPLE

The signature of $t\bar{t}$ dilepton events consists of two large transverse momentum leptons (e or μ), large missing transverse energy ($\not\!\!E_T$), two jets originating from b quarks, and possible additional jets from initial and final state radiation. We select dilepton events from inclusive high-P_T electron and muon triggers using the standard CDF lepton+track algorithm, as described in the next sections.

The main expected background processes in the dilepton sample are W+jets with a jet misidentified as a lepton ("fakes"), Drell-Yan ($Z/\gamma^* \rightarrow e^+e^-, \mu^+\mu^-, \tau^+\tau^-$), and diboson events ($WW$, WZ, ZZ) with additional jets. In the case of Drell-Yan, non-physical $\not\!\!E_T$ can be faked by mis-measured jets or leptons. The contribution of these processes to the selected data sample is reduced by optimized selection cuts.

A. Trigger

A high-transverse-momentum lepton is required by the trigger. For a central electron candidate, an electromagnetic calorimeter cluster with $E_T \equiv E \cdot \sin\theta \geq$ 18 GeV, accompanied by a matched COT track with $P_T \equiv P \cdot \sin\theta \geq 9$ GeV/c, is required. For an electron in the plug region ($1.1 < |\eta| < 2.0$), the trigger requires an electromagnetic cluster in the calorimeter with $E_T \geq 20$ GeV and $\not\!\!E_T \geq 15$ GeV. For muon candidates two or more hits in the outer muon chambers matching a track of $P_T \geq 18$ GeV/c in the central tracker are required.

B. Leptons

The LTRK selection aims at selecting two charged leptons of opposite charge with a greater acceptance than if tight lepton selection cuts were applied on both leptons. One lepton ("tight lepton") must have a well-measured track reconstructed from the interaction point with associated hits in the COT and SVX. For muons, the track is required to be compatible with hits in the muon chambers and to have $P_T > 20$ GeV/c and $|\eta| < 1$. For forward electrons a calorimetry-seeded tracking algorithm is used to identify tracks since the plug region is not well covered by the COT. In the case of electrons, the track is required to point to an electromagnetic cluster with $E_T > 20$ GeV and $|\eta| < 2$. Tight leptons must also satisfy an isolation requirement, i.e. the additional E_T in a cone of radius $\Delta R = \sqrt{\Delta\eta^2 + \Delta\phi^2} = 0.4$ about the lepton trajectory must not exceed 10% of the lepton E_T.

The other lepton ("track lepton") is required to be a well-measured track originating at the interaction point with $|\eta| < 1$ and $P_T > 20$ GeV/c. The track lepton must be isolated, which means that the ratio between the additional transverse momentum of tracks in a $\Delta R = 0.4$ cone around the track lepton and the overall P_T in the cone is less than 10%. Compared to the dilepton selection ("DIL" [19]) LTRK relaxes the calorimeter constraints on the track lepton in order to recover those events in which a lepton hits a detector crack. We refer to [6] for a more detailed comparison between LTRK and DIL.

C. Jets

Jets are the final products of quark hadronization. They are identified by looking for clusters of energy in the calorimeter using the JETCLU cone algorithm [20]. The jet search is seeded by towers with $E_T > 1$ GeV. Starting from the most energetic seed, all seeds within a 7×7 bins wide area around the seed are grouped into a cluster and the centroid is calculated. Seeds cannot belong to more than one cluster. All towers with $E_T > 0.1$ GeV within a $\Delta R = 0.4$ cone about the cluster centroid are added to the cluster and the centroid is recalculated. The procedure is iterated and a final step of splitting and merging is performed in order not to include the same tower in more than one jet.

Jet transverse energy is corrected for non-uniformities in the calorimeter response as a function of jet η, multiple $p\bar{p}$ interactions, and the hadronic jet energy scale of the calorimeter [21]. Events are required to have two or more jets with $E_T > 20$ GeV and $|\eta| < 2$.

D. Missing Transverse Energy

The definition of the uncorrected missing transverse energy is:

$$\overrightarrow{\not\!\!E_T} = -\sum_i E_T^i \hat{n}_i \qquad (1)$$

where the sum is performed over all towers with a deposited energy of at least 0.1 GeV. $\hat{n}_i$ is the transverse unit vector pointing from the CDF geometrical center to the i^{th} tower.

$\overrightarrow{\not\!\!E_T}$ is corrected to compensate for the following effects:

- the interaction vertex displacement with respect to the CDF geometrical center: $\overrightarrow{\not\!\!E_T}$ is recalculated with $\hat{n}_i$ (Eq. 1) as having the origin in the interaction point.
- potential jet mis-measurement: if a track within the jet cone has a transverse momentum larger than the jet trasnverse energy, the difference between the P_T of the highest-P_T track and the jet E_T is added to $\overrightarrow{\not\!\!E_T}$.
- muons: to correct $\overrightarrow{\not\!\!E_T}$ for the identified muons and to account for their minimum ionization contribution in the calorimeters, the difference between muon calorimeter E_T and muon P_T is added to $\overrightarrow{\not\!\!E_T}$.
- jet corrections: $\overrightarrow{\not\!\!E_T}$ is updated according to the corrections applied to the jet transverse energies, as explained above.

After corrections are applied the magnitude of the missing transverse energy is required to be larger than 25 GeV.

E. Final Selection Cuts

Several topological vetoes are implemented in order to reduce the impact of backgrounds in the sample. Background contributions from Z boson decays yielding overestimated $\not\!\!E_T$ are removed by raising the $\not\!\!E_T$ requirement to 40 GeV and the invariant mass of the tight lepton+track lepton pair to be inside the Z mass window ([76, 106] GeV/c^2). Large azimuthal separations between the $\overrightarrow{\not\!\!E_T}$ and jets ($\Delta\phi > 25°$), tight lepton ($\Delta\phi > 5°$), and track lepton ($\Delta\phi > 5°$, $\Delta\phi < 175°$) are required. These requirements have been implemented in order to reduce the number of events where mis-measured leptons or jets lead to overestimated $\not\!\!E_T$, mostly contributed by the Drell-Yan process. A lower cut on the angle between the tight lepton and $\overrightarrow{\not\!\!E_T}$ is applied to reduce the acceptance for $Z/\gamma^* \to \mu\mu$ as electron+track, where high-P_T muons are misidentified as electrons because of the emission of bremsstrahlung photons. The requirement of a minimum azimuthal angle between jets and $\overrightarrow{\not\!\!E_T}$ is dropped if $\not\!\!E_T > 50$ GeV, since such large values of missing transverse energy are not expected to arise from jet mis-measurements.

Events with muons from cosmic rays or electrons originating from the conversion of photons are removed. Cosmic muons are identified by requiring a delayed coincidence of the particle hits in the calorimeter [22]. Conversions are identified by pairing the electron track to an opposite sign track originating from a common vertex [22].

F. Sample Composition

Table II summarizes the $t\bar{t}$ signal and background rates expected for a LTRK sample corresponding to an integrated luminosity of 2.9 fb^{-1}. Depending on the process, background rates are estimated using simulated or data events. Simulated events are generated with the PYTHIA [23] Monte Carlo program, which employs CTEQ5L [24] parton distribution functions, leading-order QCD matrix elements for the hard process simulation, and parton showering to simulate fragmentation and gluon radiation. A full simulation of the CDF II detector [25] is applied. Diboson and $Z/\gamma^* \to \tau^+\tau^-$ rates are estimated with simulated events, while $Z/\gamma^* \to e^+e^-, \mu^+\mu^-$ rates are estimated with a mixture of data and simulation. We use $Z/\gamma^* \to e^+e^-, \mu^+\mu^-$ simulated events to predict the ratio of events in different kinematic regions, while we use data to normalize the overall rates. The expected fakes from W+jets and $t\bar{t}$ single lepton events with a jet misidentified as a lepton are estimated with W+jets data [26]. Signal acceptance and expected rate are evaluated using simulated $t\bar{t}$ events with a cross-section of 6.7 pb [27] and a top quark mass of 175 GeV/c^2.

TABLE II: Expected numbers of $t\bar{t}$ signal and background events with statistical uncertainties for the LTRK data sample. A $t\bar{t}$ cross-section of 6.7 pb at a top quark mass of 175 GeV/c^2 is assumed.

Process	Expected number
Signal ($t\bar{t}$)	162.6 ± 5.1
WW	10.5 ± 1.0
WZ	3.8 ± 0.3
ZZ	0.9 ± 0.1
$Z/\gamma^* \to e^+e^-$	20.8 ± 6.0
$Z/\gamma^* \to \mu^+\mu^-$	9.1 ± 3.1
$Z/\gamma^* \to \tau^+\tau^-$	19.6 ± 2.4
Fakes	80.2 ± 15.7
Total background	145.0 ± 17.3

IV. MASS RECONSTRUCTION

In this section we describe the procedure to reconstruct an event-by-event preferred top quark mass (m_t^{reco}). In the next sections we will explain how the m_t^{reco} distribution is used to extract the top quark mass.

A. Kinematics in the Dilepton Channel

To reconstruct the $t\bar{t}$ event one needs to get 4-momenta for six final state particles, 24 values in total. These final state particles are two leptons and two neutrinos from W's decays, as well as two jets originated from the top-decay b quarks. Out of the 24 final quantities, 16 (jet and lepton 4-momenta) are measured, two ($\overrightarrow{\not\!\!E_T}$ components in the transverse plane) are obtained by assuming overall transverse momentum conservation, and five constraints are imposed on the involved particle masses ($m_{W^-} = m_{W^+} = m_W$, where $m_W = 80.4$ GeV/c^2 [3], $m_t = m_{\overline{t}}$, $m_\nu = m_{\overline{\nu}} = 0$). The event kinematics is therefore under-constrained. One must assume that at least one more parameter is known in order to reconstruct the kinematics and solve for the top quark mass.

B. Neutrino ϕ Weighting Method

The method implemented in this work for reconstructing the top quark mass event by event is called "Neutrino ϕ Weighting Method". This method was previously described in [6]. In order to constrain the kinematics a scan over the space of possibilities for the azimuthal angles of the neutrinos ($\phi_{\nu_1}, \phi_{\nu_2}$) is used. A top quark mass is reconstructed by minimizing a chi-squared function (χ^2) in the dilepton $t\bar{t}$ event hypothesis. The χ^2 has two terms:

$$\chi^2 = \chi^2_{reso} + \chi^2_{constr} \tag{2}$$

The first term takes into account the detector uncertainties, whereas the second one constrains the parameters to the known physical quantities within their uncertainties. The first term is as follows:

$$\begin{aligned}\chi^2_{reso} = &\sum_{l=1}^{2} \frac{(P_T^l - \tilde{P_T^l})^2}{{\sigma_{P_T^l}}^2} - 2\sum_{j=1}^{2} \ln(\mathscr{P}_{tf}(\tilde{P_T^j}|P_T^j)) \\ &+ \sum_{i=x,y} \frac{(E_U^i - \tilde{E_U^i})^2}{{\sigma_{E_U^i}}^2}\end{aligned} \tag{3}$$

With the use of the tilde ($\sim$) we specify the parameters of the minimization procedure, whereas variables without tilde represent the measured values. $\mathscr{P}_{tf}$ are the transfer functions between b quark and jets: they express the probability of measuring a jet transverse momentum P_T^j from a b quark with transverse momentum $\tilde{P_T^j}$. We will comment on $\mathscr{P}_{tf}$ in Section IV C. The sum in the first term is over the two leptons in the event; the second sum loops over the two highest-E_T (leading) jets, which are assumed to originate from the b quarks (this assumption is true in about 70% of simulated $t\bar{t}$ events [6]).

The third sum in Eq. 3 runs over the transverse components of the unclustered energy (E_U^x, E_U^y), which is defined as the sum of the energy vectors from the towers not associated with leptons or any leading jets. It also includes possible additional jets with $E_T > 8$ GeV within $|\eta| < 2$.

The uncertainties (σ_{P_T}) on the tight lepton P_T used for identified electrons (e) and muons (μ) are calculated as [6]:

$$\frac{\sigma^e_{P_T}}{P^e_T} = \sqrt{\frac{0.135^2}{P^e_T[\text{GeV}/c]} + 0.02^2} \tag{4}$$

$$\frac{\sigma^\mu_{P_T}}{P^\mu_T} = 0.0011 \cdot P^\mu_T[\text{GeV}/c] \tag{5}$$

The track-lepton momentum uncertainty is calculated as for the muons, since momentum is measured in the tracker for both electrons and muons. Uncertainty for the transverse components of the unclustered energy, σ_{E_U}, is defined as $0.4\sqrt{E_T^{\text{uncl}}}$[GeV] [28], where E_T^{uncl} is the scalar sum of the transverse energy excluding the two leptons and the two leading jets.

The second term in Eq. 2, χ^2_{constr}, constrains the parameters of the minimization procedure through the invariant masses of the lepton-neutrino and of the lepton-neutrino–leading-jet systems. This term is as follows:

$$\begin{aligned}\chi^2_{constr} = &-2\ln(\mathscr{P}_{BW}(m_{inv}^{l_1,\nu_1}|m_W,\Gamma_{m_W})) \\ &-2\ln(\mathscr{P}_{BW}(m_{inv}^{l_2,\nu_2}|m_W,\Gamma_{m_W})) \\ &-2\ln(\mathscr{P}_{BW}(m_{inv}^{l_1,\nu_1,j_1}|\tilde{m}_t,\Gamma_{\tilde{m}_t})) \\ &-2\ln(\mathscr{P}_{BW}(m_{inv}^{l_2,\nu_2,j_2}|\tilde{m}_t,\Gamma_{\tilde{m}_t}))\end{aligned} \tag{6}$$

$\tilde{m}_t$ is the parameter giving the reconstructed top quark mass. $\mathscr{P}_{BW}(m_{inv};\ m,\Gamma) \equiv \frac{\Gamma^2 \cdot m^2}{(m^2_{inv} - m^2)^2 + m^2\Gamma^2}$ indicates the relativistic Breit-Wigner distribution function,

which expresses the probability that an unstable particle of mass m and decay width Γ decays into a system of particles with invariant mass m_{inv}. We use the PDG [3] values for m_W and Γ_{m_W}. For the top width we use the function

$$\Gamma_{m_t} = \frac{G_F}{8\sqrt{2}\pi} m_t^3 (1 - \frac{m_W^2}{m_t^2})^2 (1 + 2\frac{m_W^2}{m_t^2}) \qquad (7)$$

according to Ref. [29]. This new formulation of the χ^2_{constr} term helps to decrease the statistical error of the top mass reconstruction by 20%.

The longitudinal components of the neutrino momenta are free parameters of the minimization procedure, while the transverse components are related to $\overrightarrow{\not\!\!E_T}$ and to the assumed $(\phi_{\nu_1}, \phi_{\nu_2})$ as follows:

$$\begin{cases} P_x^{\nu_1} \equiv P_T^{\nu_1} \cdot \cos(\phi_{\nu_1}) = \\ \quad \frac{\not\!\!E_{Tx} \cdot \sin(\phi_{\nu_2}) - \not\!\!E_{Ty} \cdot \cos(\phi_{\nu_2})}{\sin(\phi_{\nu_2} - \phi_{\nu_1})} \cdot \cos(\phi_{\nu_1}) \\ P_y^{\nu_1} \equiv P_T^{\nu_1} \cdot \sin(\phi_{\nu_1}) = \\ \quad \frac{\not\!\!E_{Tx} \cdot \sin(\phi_{\nu_2}) - \not\!\!E_{Ty} \cdot \cos(\phi_{\nu_2})}{\sin(\phi_{\nu_2} - \phi_{\nu_1})} \cdot \sin(\phi_{\nu_1}) \\ P_x^{\nu_2} \equiv P_T^{\nu_2} \cdot \cos(\phi_{\nu_2}) = \\ \quad \frac{\not\!\!E_{Tx} \cdot \sin(\phi_{\nu_1}) - \not\!\!E_{Ty} \cdot \cos(\phi_{\nu_1})}{\sin(\phi_{\nu_1} - \phi_{\nu_2})} \cdot \cos(\phi_{\nu_2}) \\ P_y^{\nu_2} \equiv P_T^{\nu_2} \cdot \sin(\phi_{\nu_2}) = \\ \quad \frac{\not\!\!E_{Tx} \cdot \sin(\phi_{\nu_1}) - \not\!\!E_{Ty} \cdot \cos(\phi_{\nu_1})}{\sin(\phi_{\nu_1} - \phi_{\nu_2})} \cdot \sin(\phi_{\nu_2}) \end{cases} \qquad (8)$$

The minimization procedure described above must be performed for all the allowed values of ϕ_{ν_1}, ϕ_{ν_2} in the $(0, 2\pi) \times (0, 2\pi)$ region. Based on simulation, we choose a ϕ_{ν_1}, ϕ_{ν_2} grid of 24×24 values as inputs for the minimization procedure. In building the grid we avoid the singular points at $\phi_{\nu_1} = \phi_{\nu_2} + k \cdot \pi$, where k is integer. For these points, which correspond to a configuration where the two neutrinos are collinear in transverse plane, the kinematics of the event cannot be reconstructed using Eqs. 3- 8. Avoiding these points in our procedure does not effect the reconstruction of the top mass central value, but rather effects the width of the mass distribution per event. Note from Eq. 8 that performing the transformation $\phi_\nu \to \phi_\nu + \pi$ leaves P_x^ν and P_y^ν unchanged, but reverses the sign of P_T^ν. We exclude unphysical solutions ($P_T^{\nu_1} < 0$ and/or $P_T^{\nu_2} < 0$) and choose the solution which leads to positive transverse momenta for both neutrinos. This decreases the number of grid points to 12×12. At each point 8 solutions can exist, because of the two-fold ambiguity in the longitudinal momentum for each neutrino and of the ambiguity on the lepton-jet association. Therefore, for each event, we perform 1152 minimizations, each of which returns a value of m_{ijk}^{reco} and χ^2_{ijk} ($i, j = 1, \ldots, 12$; $k = 1, \ldots, 8$). We define $\chi'^2_{ij} = \chi^2_{ij} + 4 \cdot \ln(\Gamma_{m_t})$, which is obtained by using Eq. 6 where $\mathscr{P}_{BW}$ is substituted with $\frac{\Gamma \cdot m^2}{(m^2_{inv} - m^2)^2 + m^2\Gamma^2}$, and select the lowest χ'^2 solution for each point of the $(\phi_{\nu_1}, \phi_{\nu_2})$ grid, thereby reducing the number of obtained masses to 144. Each mass is next weighted according to

$$w_{ij} = \frac{e^{-\chi'^2_{ij}/2}}{\sum_{i=1}^{12} \sum_{j=1}^{12} e^{-\chi'^2_{ij}/2}} \qquad (9)$$

A top quark mass distribution is built in order to identify the most probable value (MPV) for the event. Based on a result of the simulation, the following procedure for improving the performance of solution-weighting was implemented. Masses below a threshold of 30% the MPV bin content are discarded, and the remaining ones are averaged to compute the preferred top quark mass for the event.

C. Transfer Functions

Since jet energy corrections have been calibrated on samples dominated by light quarks and gluons, we need an additional correction for a better reconstruction of the energy of b-quark jets. In Equation 3, we introduced the transfer functions $\mathscr{P}_{tf}$, which allow us to step back from jets to partons. These functions of jet η and P_T are defined as the parameterization of $\xi \equiv (P_T^{b-quark} - P_T^{jet})/P_T^{jet}$ distributions, built from a large sample of simulated $t\bar{t}$ events. The b-quark jets in the simulation are recognized using true MC information. Jets with axis within a $R = 0.4$ cone about the generated b quarks are used. The influence of b-quark P_T spectra on the ξ distributions is minimized by choosing the weights inversely proportional to the probability density of $P_T^{b-quark}$. Also, this greatly reduces dependence of the transfer functions on m_t.

In order to parameterize the above distributions we found the following expression to be adequate:

$$\begin{aligned} \mathscr{W}_{TF}(\xi) = & \frac{\gamma_7\gamma_6}{\sqrt{2\pi}\gamma_2} \, e^{-0.5(\frac{\xi-\gamma_1}{\gamma_2} + \exp(-\frac{\xi-\gamma_1}{\gamma_2}))} \\ & + \frac{\gamma_7(1-\gamma_6)}{\sqrt{2\pi}\gamma_5} \, e^{-0.5(\frac{\xi-\gamma_4}{\gamma_5})^2} \\ & + \frac{(1-\gamma_7)}{\sqrt{2\pi}\gamma_3} \, e^{-0.5(\frac{\xi-\gamma_8}{\gamma_3})^2} \end{aligned} \qquad (10)$$

The parameters $\gamma_1 \cdots \gamma_8$ are derived from the fit. The distributions are built for three $|\eta|$ regions: $|\eta| < 0.7$, $0.7 < |\eta| < 1.3$, and $1.3 < |\eta| < 2.0$.

Figure 2 shows the distributions and the transfer functions for a number of $(|\eta|, P_T^{jet})$ regions. 10 GeV/c wide P_T bins are used from 30 GeV/c to 190 GeV/c for $|\eta| < 0.7$, from 30 GeV/c to 150 GeV/c for $0.7 < |\eta| < 1.3$, and from 30 GeV/c to 110 GeV/c for $1.3 < |\eta| < 2.0$. A single bin is used above and below these regions.

V. TOP QUARK MASS DETERMINATION

The selected data sample is a mixture of signal and background events. In order to extract the top quark

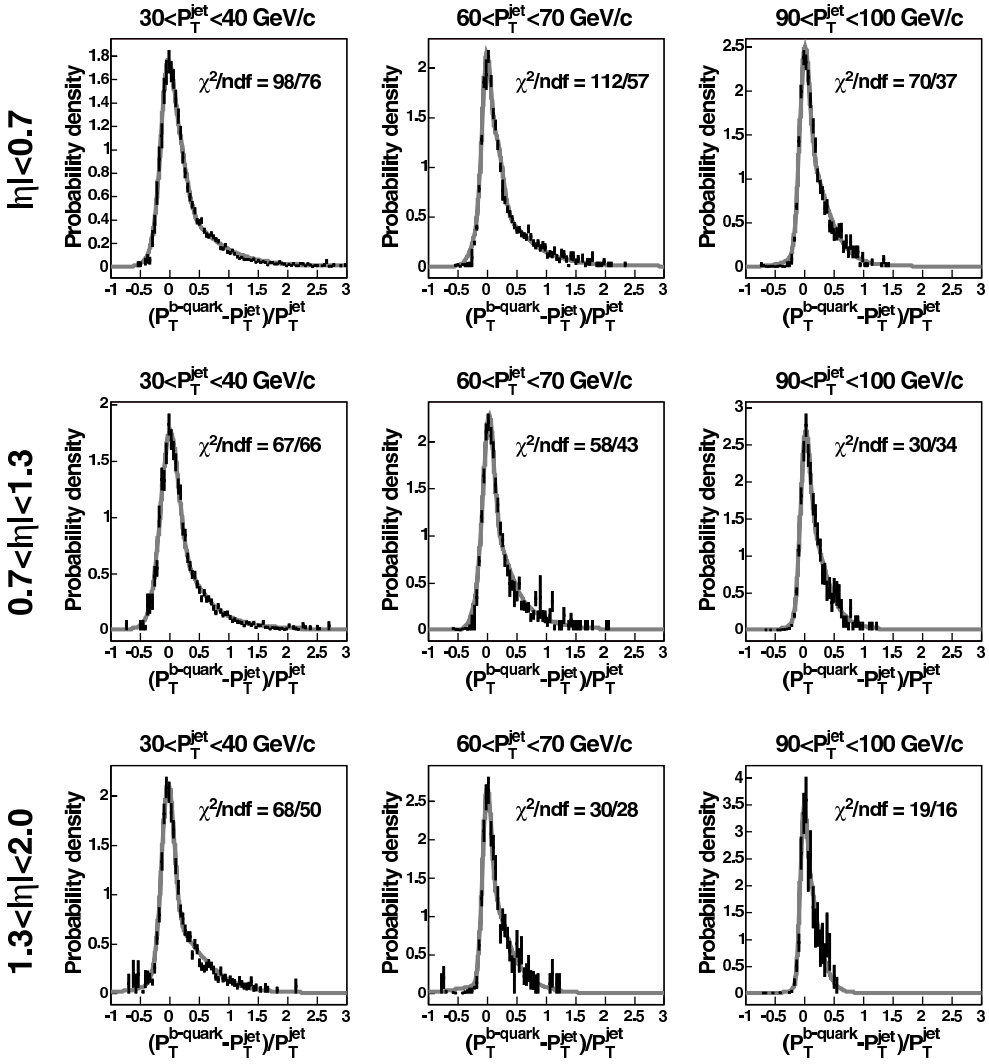

FIG. 2: Examples of the transfer functions of b quarks into jets used in the fit. These functions of jet η and P_T are defined as the parameterization of $(P_T^{b-quark} - P_T^{jet})/P_T^{jet}$ distributions. The points are from the simulated $t\bar{t}$ events. The curves show the parameterization with Eq. 10.

mass, the reconstructed top quark mass distribution in data is compared with probability density functions (p.d.f.'s) for signal and background by means of a likelihood minimization. P.d.f.'s are defined as the parameterizations of m_t^{reco} templates obtained by applying the neutrino ϕ weighting method on simulated signal and background events, which are selected according to the lepton+track algorithm.

A. Templates

Signal templates are built from $t\bar{t}$ samples generated with PYTHIA for top quark masses in the range 155 to 195 GeV/c^2 in 2 GeV/c^2 steps. They are parameterized in a global fit by using a combination of one Landau and two Gaussian distribution functions, as:

$$P_s(m_t^{reco}|m_t) = \frac{c_1 p_6}{\sqrt{2\pi}p_2}\, e^{-0.5(\frac{m_t^{reco}-p_1}{p_2}+\exp(-\frac{m_t^{reco}-p_1}{p_2}))} + \frac{c_1(1-p_6)}{\sqrt{2\pi}p_5}\, e^{-0.5(\frac{m_t^{reco}-p_4}{p_5})^2} + \frac{(1-c_1)}{\sqrt{2\pi}p_3}\, e^{-0.5(\frac{m_t^{reco}-c_2}{p_3})^2} \quad (11)$$

P_s, the signal p.d.f., expresses the probability that a mass m_t^{reco} is reconstructed from an event with true top quark mass m_t. The constants c_1 and c_2 are set a-priori to adhere to the features of the template shape. The parameters $p_1, \ldots, p_6$ depend on the true top quark mass m_t are calculated as:

$$p_k = \alpha_k + \alpha_{k+6} \cdot (m_t[\mathrm{GeV}/c^2] - 175) \quad k = 1, \ldots, 6 \quad (12)$$

The parameters α_k are obtained from the fit to the signal templates. Figure 3 shows a subset of templates along with their parameterizations (solid lines).

A representative background template is built by adding fakes, Drell-Yan, and diboson templates. These templates have been normalized to the expected rates reported in Table II. The fakes template is built from W+jets data events by weighting each event according to the probability for a jet to be mis-identified as a lepton (fake rate) [26]. Drell-Yan and diboson templates are built from samples simulated with PYTHIA and ALPGEN [30] + PYTHIA respectively. The combined background template is fitted with a sum of two Landau and one Gaussian distribution functions, as:

$$\begin{aligned} P_b(m_t^{reco}) = & \frac{k_1\beta_6}{\sqrt{2\pi}\beta_2}\ e^{-0.5(\frac{m_t^{reco}-\beta_1}{\beta_2}+\exp(-\frac{m_t^{reco}-\beta_1}{\beta_2}))} \\ & + \frac{k_1(1-\beta_6)}{\sqrt{2\pi}\beta_5}\ e^{-0.5(\frac{m_t^{reco}-\beta_4}{\beta_5})^2} \\ & + \frac{(1-k_1)}{\sqrt{2\pi}\beta_3}\ e^{-0.5(\frac{m_t^{reco}-k_2}{\beta_3}+\exp(-\frac{m_t^{reco}-k_2}{\beta_3}))} \end{aligned} \quad (13)$$

where the fit parameters $\beta_1 \cdots \beta_6$ are m_t-independent. The constants k_1 and k_2 are set a-priori to adhere to the features of the template shape. The combined background template and its parameterization (solid line), Drell-Yan, diboson, and fakes templates are plotted in Figure 4.

B. Likelihood Minimization

The top quark mass estimator is extracted from the data sample by performing an unbinned likelihood fit and minimization. The likelihood function expresses the probability that a m_t^{reco} distribution from data is described by a mixture of background events and dilepton $t\bar{t}$ events with an assumed top quark mass. Inputs for the likelihood fit are the reconstructed mass (m_n), the simulated signal and background p.d.f.'s, and the expected background. The background expectation (n_b^{exp}=145.0) and its uncertainty ($\sigma_{n_b^{exp}}$=17.3) are taken from Table II. The likelihood takes the form:

$$\mathscr{L} = \mathscr{L}_{shape} \cdot \mathscr{L}_{backgr} \cdot \mathscr{L}_{param}; \quad (14)$$

where

$$\begin{aligned} \mathscr{L}_{shape} = & \frac{e^{-(n_s+n_b)} \cdot (n_s+n_b)^N}{N!} \\ & \cdot \prod_{n=1}^{N} \frac{n_s \cdot P_s(m_n|m_{top}) + n_b \cdot P_b(m_n)}{n_s+n_b}, \end{aligned} \quad (15)$$

$$\mathscr{L}_{backgr} = \exp(\frac{-(n_b-n_b^{exp})^2}{2\sigma^2_{n_b^{exp}}}) \quad (16)$$

and

$$\begin{aligned} \mathscr{L}_{param} = \exp\{-0.5[&(\vec{\alpha}-\vec{\alpha_0})^T U^{-1}(\vec{\alpha}-\vec{\alpha_0}) \\ &+ (\vec{\beta}-\vec{\beta_0})^T V^{-1}(\vec{\beta}-\vec{\beta_0})]\}. \end{aligned} \quad (17)$$

The top quark mass estimator (m_{top}) returned by the minimization is the mass corresponding to $[-\ln\mathscr{L}]_{min}$. The shape likelihood term, $\mathscr{L}_{shape}$ (Eq. 15), expresses the probability of an event being signal with the top mass m_{top} or background. The signal (P_s) and background (P_b) probabilities are weighted according to the number of signal (n_s) and background (n_b) events, which are floated in the likelihood fit. In the fitting procedure, n_b is constrained to be Gaussian-distributed with mean value n_b^{exp} and standard deviation $\sigma_{n_b^{exp}}$, as shown in Eq. 16, while (n_s+n_b) is the mean of a Poisson distribution of N selected events. In this manner, the number of signal events is independent of the expected $t\bar{t}$ lepton+track events in a particular assumption of the $t\bar{t}$ cross-section value. $\mathscr{L}_{param}$ constrains the parameters of the signal ($\vec{\alpha}$) (see Eq. 12) and background ($\vec{\beta}$) (see Eq. 13) p.d.f.'s. These p.d.f.'s have Gaussian distribution with mean values ($\vec{\alpha}_0$) and ($\vec{\beta}_0$) obtained from the signal and background templates fit. U and V are the corresponding covariant matrices for $\vec{\alpha}$ and $\vec{\beta}$ returned from the MINUIT [31] minimization.

VI. CALIBRATION OF THE METHOD

The method described above is calibrated in order to avoid systematic biases in the measured top quark mass and in its uncertainty. Calibrations are performed by running a large number (10^4) of "pseudo-experiments" (PE's) on simulated background and signal events where the true top quark mass is known. Each PE consists of determining the number of signal (N_s^{PE}) and background (N_b^{PE}) events in the sample, drawing N_s^{PE} masses from a signal template and N_b^{PE} from the background template, and fitting the mass distribution to a combination of signal and background p.d.f.'s, as described in Section V. A top quark mass (m_t^{fit}) and its positive and negative statistical uncertainties (σ^+ and σ^-) are returned by the fit. Numbers of signal and background events are generated according to Poisson distributions with means given in Table II.

For each input top quark mass the median of the m_t^{fit} distribution is chosen as the mass estimate (m_t^{out}). The distributions of m_t^{out} versus input mass (m_t) and the bias, defined as $\Delta M = m_t^{out} - m_t$, are shown in Figure 5. The uncertainty bars are determined by the limited statistics of the signal and background templates. Both fits in Figure 5 are performed in the mass range 159-191 GeV/c^2. The slope of the straight line in the upper plot is consistent with one, while the average bias (horizontal line in the lower plot) is -0.13 ± 0.10 GeV/c^2. Although this value can be considered compatible with zero within un-

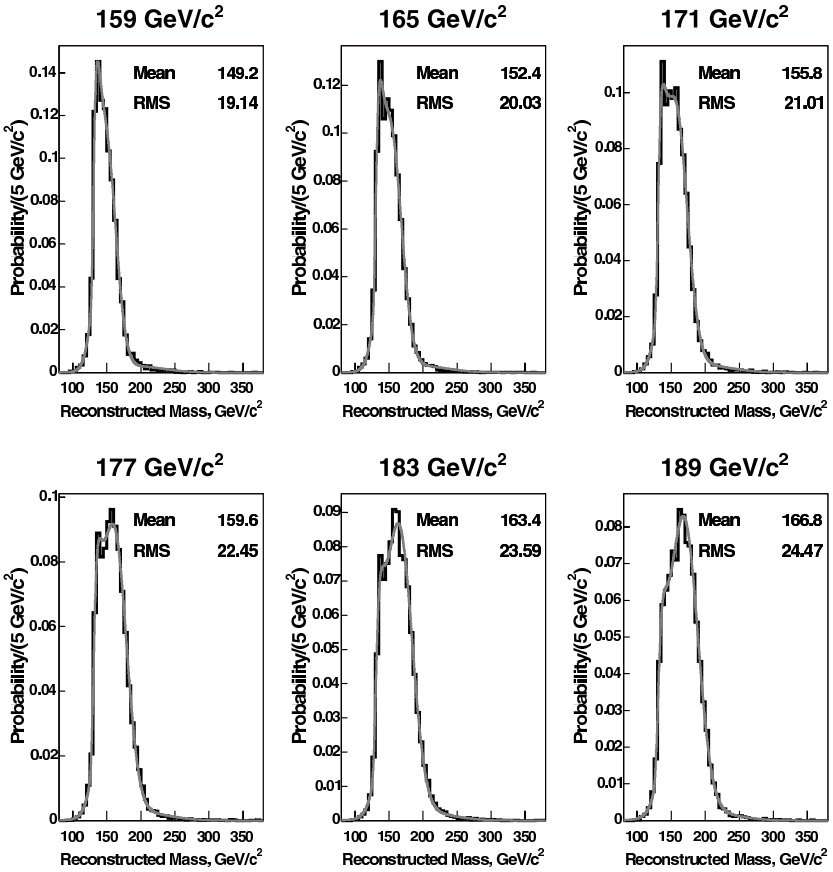

FIG. 3: Signal templates and fitting functions (solid lines) for a number of generated top quark masses. The parameterization is defined in Eq. 11.

certainties, we apply a shift of $+0.13\,\mathrm{GeV}/c^2$ to the result on data.

In order to check the bias on the statistical uncertainty we use pull distributions, defined as follows:

$$\mathrm{pull} = \frac{m_t^{fit} - m_t}{\sigma'} \tag{18}$$

where $\sigma' = \begin{cases} \sigma^+ \text{ if } m_t^{fit} < m_t \\ |\sigma^-| \text{ if } m_t^{fit} > m_t \end{cases}$. The positive and negative statistical uncertainties are returned by MINUIT (routine MINOS) [31]. For each generated top quark mass, pull distributions are fitted by Gaussian functions (some examples are shown in Figure 6).

The mean and width of the pull distributions versus generated top quark mass are shown in Figure 7. Error bars account for the limited statistics of signal and background templates. The average width of pull distributions is 1.009 ± 0.005. A width larger than one indicates an underestimate of the statistical uncertainty. Accordingly, the statistical uncertainty obtained from data is increased by a factor 1.009.

VII. RESULTS

The data sample used in this measurement corresponds to an integrated luminosity of 2.9 fb^{-1}. A total of 328 LTRK candidates are found in data. Selected events are reconstructed and an experimental mass distribution is built. The likelihood constrained fit described in Section V B is performed and the following estimate of the top quark mass with statistical uncertainties is obtained:

$$m_{top} \;=\; 165.35^{+3.35}_{-3.22}\ \mathrm{GeV/c^2} \tag{19}$$

The experimental top quark mass distribution is shown in Figure 8. The constrained fit returns $181.4^{+21.9}_{-21.3}$ signal and $146.1^{+15.1}_{-15.0}$ background events. The observed rates are in good agreement with expectations (Table II).

As a check, we remove the Gaussian constraint on the number of background events in Formula 14. The unconstrained fit returns:

$$m_{top} \;=\; 165.33^{+3.39}_{-3.28}\ \mathrm{GeV}/c^2 \tag{20}$$

with $178.6^{+30.9}_{-31.1}$ signal and $149.4^{+31.6}_{-29.5}$ background events. The top quark mass and the number of signal and background events from unconstrained and constrained fits are in agreement.

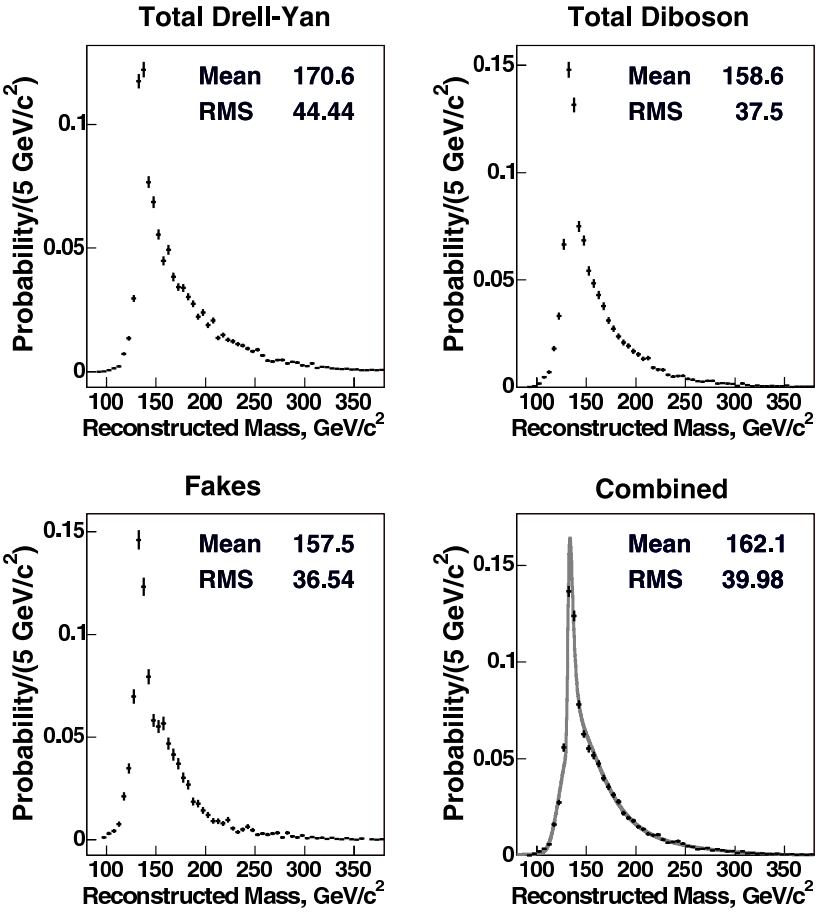

FIG. 4: Drell-Yan, fakes, diboson and combined background templates. The fitting function (solid line), defined in Eq. 13, is superimposed to the combined template.

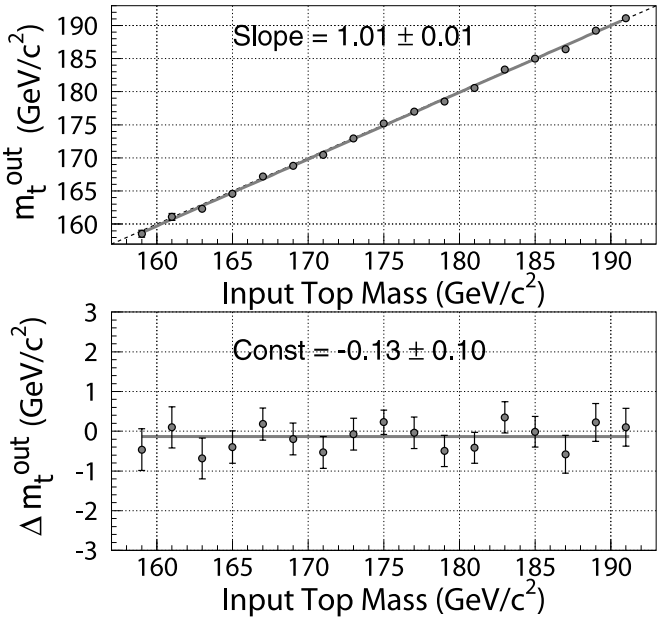

FIG. 5: Results from pseudo-experiments. The upper plot shows m_t^{out} versus input masses, while the lower one shows the bias.

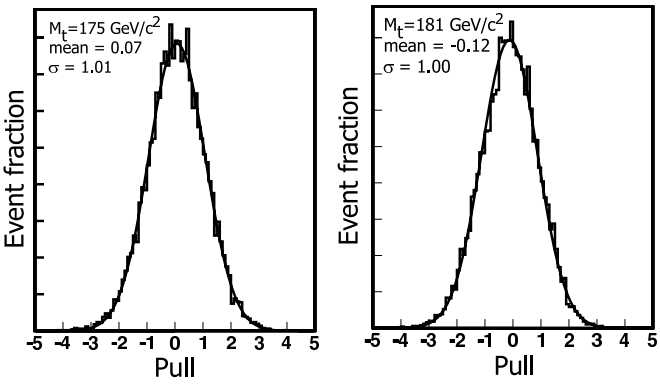

FIG. 6: Results from pseudo-experiments: pull distributions for generated mass samples at $m_t = 175$ GeV/c^2 (left) and $m_t = 181$ GeV/c^2 (right). Distributions are fitted to Gaussian functions (solid line), returning the indicated means and standard deviations.

The top quark mass and its statistical uncertainty obtained from the constrained fit (Eq. 19) are corrected for the expected systematic 0.13 GeV/c^2 shift, and for the 1.009 width of the pull distribution (Section VI) respec-

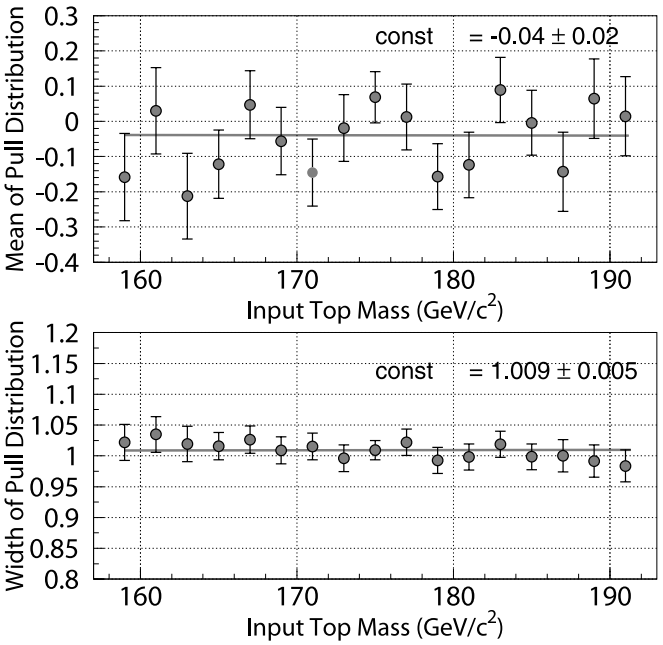

FIG. 7: Results from pseudo-experiments: mean and width of the pull distributions versus generated top quark mass are shown in the upper and lower plots respectively.

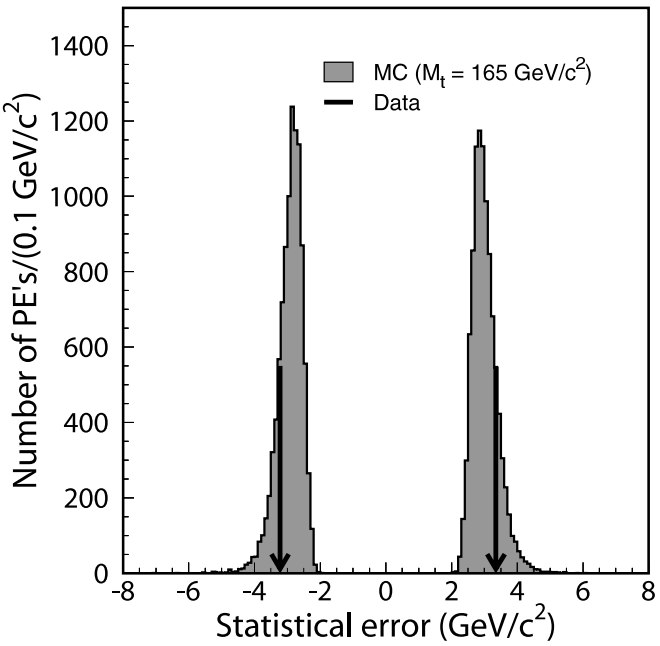

FIG. 9: Expected statistical uncertainties from pseudo-experiments generated with a top quark mass of 165 GeV/c^2. The arrows indicate the uncertainties found in this measurement.

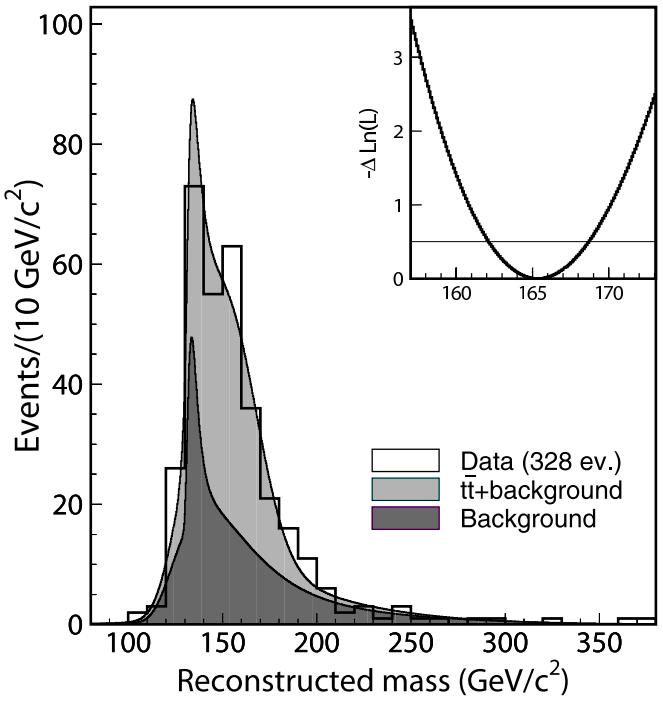

FIG. 8: Two-component constrained fit to the 328-event LTRK data sample. Background (dark gray) and signal+background (light gray) p.d.f.'s, normalized according to the numbers returned by the fit, are superimposed to the reconstructed mass distribution from data (histogram). The insert shows the fitted mass-dependent negative log-likelihood function.

tively. The final value is:

$$m_{top} = 165.5^{+3.4}_{-3.3}(\text{stat.})\ \text{GeV}/c^2 \quad (21)$$

In order to check that the measured statistical uncertainty is reasonable, a set of PE's is performed on simulated background and signal events with $m_t = 165$ GeV/c^2 (close to the central value of the constrained fit), as explained in Section VI. The obtained positive and negative error distributions along with the observed values (arrows) are shown in Figure 9. We found that the probability for obtaining a precision better than that found in this experiment is 82%.

VIII. SYSTEMATIC UNCERTAINTIES

Since our method compares findings to expectations estimated from Monte Carlo simulations, uncertainties in the models used to generate events cause systematic uncertainties. Other systematic uncertainties arise from the potential mis-modeling of the background template shape.

The procedure for estimating a systematic uncertainty is as follows. The parameters used for the generation of events are modified by ± 1 standard deviation in their uncertainties and new templates are built. PE's from the modified templates are performed using the same p.d.f.'s as in the analysis. The obtained medians of the top quark mass distribution from PE's and the nominal top quark mass are used to estimate the systematic uncertainty.

The source of each systematic uncertainty is assumed to be uncorrelated to the other ones, so that the overall systematic uncertainty is obtained by adding in quadrature the individual uncertainties. The systematic uncertainties along with the total uncertainty are summarized in Table V. In the following, we describe how each systematic uncertainty is evaluated.

A. Jet energy scale

The measured jet energy is corrected according to the measured and simulated calorimeter response to electrons and hadrons [32]. Jet corrections also correct for the non-uniformities in calorimeter response as a function of $|\eta|$, effects of multiple $p\bar{p}$ collisions, the hadronic jet energy scale, deposited energy within the jet cone by the underlying events, and out-of-cone jet energy lost in the clustering procedure. The systematic uncertainty due to the jet energy scale (JES) is estimated from signal and background events in which each jet energy correction has been shifted by $\pm$ 1 standard deviation in the energy scale factor. Shifted signal and background templates are built and two sets of 10^4 PE's are performed. The systematic uncertainty for each level of corrections is taken as $(m_t^+ - m_t^-)/2$, where m_t^+ and m_t^- are the top quark masses found respectively for a lower and upper shift of the parameter. The individual uncertainties are summed in quadrature in order to obtain the JES systematic uncertainty. Results are reported in Table III. The systematic uncertainty in the top quark mass due to the JES uncertainty is 2.9 GeV/c^2.

TABLE III: Summary of jet energy scale systematic uncertainties

Source	Uncertainty (GeV/c^2)
η calorimeter non-uniformity	0.6
multiple interactions	0.0
hadronic jet energy scale	2.2
underlying event	0.2
out-of-cone energy loss	1.8
Total	2.9

Since jet energy corrections are estimated with studies dominated by light quarks and gluon jets, additional uncertainty occurs on the b-jet energy scale because of three main reasons [28]:

1. uncertainty in the heavy-flavor fragmentation model;

2. uncertainty in the b-jet semileptonic branching ratio;

3. uncertainty in the calorimeter response to energy released by b-jets.

The effect of the fragmentation model on the top quark mass is evaluated by reweighting events according to two different fragmentation models from fits on LEP [33] and SLD [34] data, while effects of the uncertainties on the semileptonic b-jet branching ratio (BR) and b-jet energy calorimeter response are estimated by shifting the BR and the b-jet energy scale. In all cases shifted templates are built and PE's are performed. The resulting shifted masses are used to estimate the systematic uncertainty due to each of the sources. These uncertainties are added in quadrature. The total systematic uncertainty in the b-jet energy scale is 0.4 GeV/c^2.

B. Lepton energy scale

The uncertainty on the lepton energy scale may affect the top quark mass measurement. This uncertainty is studied by applying a $\pm 1\%$ shift to the P_T of leptons [21]. Shifted templates are built and PE's are performed. Half of the difference of the resulting masses is taken as the systematic uncertainty on the top quark mass due to the lepton energy scale uncertainty. The systematic uncertainty in the lepton energy scale is 0.3 GeV/c^2.

C. Monte Carlo event generation

Several systematic uncertainties are due to the modeling of $t\bar{t}$ signal events.

1. *Monte Carlo generators*

The effect of the choice of a particular Monte Carlo generator is studied by comparing our default PYTHIA generator to HERWIG. These generators differ in the hadronization models, handling of the underlying $p\bar{p}$ events and of the multiple $p\bar{p}$ collisions in the same bunch crossing, and in the spin correlations in the production and decay of $t\bar{t}$ pairs (implemented in HERWIG only) [35]. The difference between masses obtained from sets of PE's performed with the two generators is found. The systematic uncertainty due to our choice of Monte Carlo generators is 0.2 GeV/c^2.

2. *Initial and final state radiation*

The effect of the initial and final state radiation (ISR and FSR) parameterization is studied, since jets radiated by interacting partons can be misidentified as leading jets and affect the top quark mass measurement. The systematic uncertainty associated with ISR is obtained by adjusting the QCD parameters in the DGLAP [36] parton shower evolution in $t\bar{t}$ events. The size of this adjustment has been obtained from comparisons between Drell-Yan data and simulated events [28]. Since the physical laws

that rule ISR and FSR are the same, the parameters that control ISR and FSR are varied together (IFSR). Half of the difference in top quark mass from PE's performed on samples with increased and decreased IFSR is taken as the systematic uncertainty for the radiation modeling. The systematic uncertainty due to uncertainties in the initial and final state radiation is 0.2 GeV/c^2.

3. PDFs

The uncertainty in reconstructing the top quark mass due to the use of sets of parton distribution function (PDF) comes from three sources: PDF choice, PDF parameterization, and QCD scale (Λ_{QCD}). The uncertainty due to the PDF choice is estimated as the difference between the top quark mass extracted by using CTEQ5L (default) and MRST72 [37]. The uncertainty due to PDF parameterization is estimated by shifting by ± 1 standard deviation one at a time the 20 eigenvectors of CTEQ6M [24]. Half of the differences between the shifted masses derived from PE's are added in quadrature. The measured mass differences between MRST72, generated with Λ_{QCD} = 300 MeV, and MRST75, generated with Λ_{QCD} = 228 MeV, [37] is taken as the uncertainty due to the choice of Λ_{QCD}. These systematic uncertainties are added in quadrature. Results are summarized in Table IV. The total systematic uncertainty due to uncertainties in the PDFs is 0.3 GeV/c^2.

TABLE IV: PDF systematic uncertainties on top quark mass. The total systematic uncertainty is the sum in quadrature of the individual contributions.

Source	Uncertainty (GeV/c^2)
PDF parameterization	0.2
PDF choice	0.1
Λ_{QCD}	0.2
Total	0.3

4. Luminosity profile (event pileup)

Pseudo-experiment simulations have only been made for a probability of multiple interactions in a single bunch crossing as appropriate for the collider luminosity during the first period of data taking (1.2 fb^{-1} integrated luminosity.) A possible discrepancy between simulation and data collected at later times at higher luminosity may affect the top quark mass measurement. We evaluate this effect by running batches of PE's on $t\bar{t}$ events, selected according to the number of interaction vertices found in the event.

The results from PE's are plotted against the number of interactions and a linear fit is applied (Figure 10). Since we do not see a significant mass dependence, we use the uncertainty (0.26 GeV/c^2/interaction) on the slope

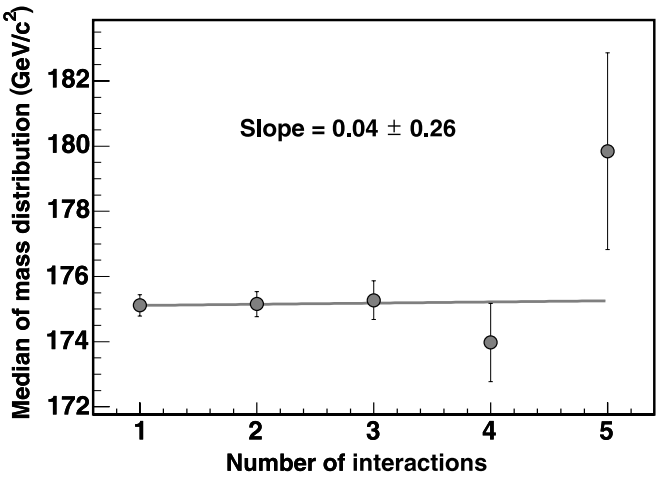

FIG. 10: Results from pseudo-experiments performed using events selected according to the number of interactions.

to derive the systematic uncertainty. We multiply 0.26 GeV/c^2/interaction by $< N_{vtx}^{data} > - < N_{vtx}^{MC} >$, where $< N_{vtx}^{data} >$=2.07 and $< N_{vtx}^{MC} >$=1.50 are the average number of vertices in the selected data sample and simulated sample respectively. We obtain a 0.15 GeV/c^2 top mass uncertainty due to the event pile-up.

D. Background template shape

The systematic uncertainties due to the potential mismodeling of the background template shape were also estimated. We identify three independent sources for this systematic uncertainty: background composition, W+jets fakes shape, and Drell-Yan shape. The effect of the diboson shape is neglected because of the small expected rate of this background (Table II).

In order to estimate the systematic uncertainty for the background composition, fakes, diboson, and Drell-Yan, the expected rates are alternatively varied by plus or minus one standard deviation (Table II) without changing the total number of expected background events. Half of the differences between $\pm$ 1 σ shifted masses derived from PE's are added in quadrature. The systematic uncertainty due to uncertainty in the background composition is 0.5 GeV/c^2.

The uncertainty on the shape of the fake background template (Section V A) is modeled. The fake rate E_T dependence is varied according to the fake rate uncertainties in each E_T bin. Two shifted background templates are built and used for PE's. The corresponding shift in mass is taken as the systematic uncertainty due to potential mis-modeling of fake shape. The top mass uncertainty due to uncertainty in the fake shape is 0.4 GeV/c^2.

Drell-Yan events with associated jets can pass the selection because jet mis-measurements can cause a large unphysical $\not\!\!E_T$. Mis-modeling of this effect is studied,

since it may affect the top quark mass measurement. Two modified Drell-Yan templates are built by re-weighting $Z/\gamma^* \to e^+e^-, \mu^+\mu^-$ events. The weight has been optimized by looking at discrepancies in $\not\!\!E_T$ between Monte Carlo simulation and data. Results of PE's performed with the modified Drell-Yan templates are used to estimate the systematic uncertainty due to the possible fluctuation in the shape of this background. The mass systematic uncertainty due to uncertainties in the shape of the Drell-Yan background is 0.3 GeV/c^2.

TABLE V: Summary of systematic uncertainties on the top quark measurement.

Source	Uncertainty (GeV/c^2)
Jet energy scale	2.9
b-jet energy scale	0.4
Lepton energy scale	0.3
Monte Carlo generators	0.2
Initial and final state radiation	0.2
Parton distribution functions	0.3
Luminosity profile (pileup)	0.2
Background composition	0.5
Fakes shape	0.4
Drell-Yan shape	0.3
Total	**3.1**

IX. CONCLUSIONS

Using the template technique on a lepton+track sample we measure a top quark mass of

$$\begin{aligned} m_{top} &= 165.5^{+3.4}_{-3.3}(\text{stat.}) \pm 3.1(\text{syst.})\ \text{GeV}/c^2 \\ &\text{or} \\ m_{top} &= 165.5^{+4.6}_{-4.5}\text{GeV}/c^2 \end{aligned} \quad (22)$$

This result agrees with the world average top quark mass ($m_{top} = 172.4 \pm 1.2$ GeV/c^2 [38]), obtained by combining the main CDF and DØ Run I (1992-1996) and Run II (2001-present) results.

Compared with our previous result ($m_{top} = 169.7 \pm 9.8$ GeV/c^2 [6]), obtained on a $\int Ldt = 340$ pb^{-1} data sample, a significant improvement in the total uncertainty has been achieved. The improvement due to the novelties in the analysis technique is estimated from PE's to be about 20%. The improvements which made this progress possible are the introduction of relativistic Breit-Wigner distribution functions in event reconstruction, along with m_{top}-dependent top width, while in [6] Gaussian distribution functions and a constant top width were used. A new feature of this analysis is the use of a larger statistics lepton+track sample which overlaps by only $\sim 45\%$ with the often used dilepton sample [6].

X. ACKNOWLEDGMENTS

We thank the Fermilab staff and the technical staffs of the participating institutions for their vital contributions. This work was supported by the U.S. Department of Energy and National Science Foundation; the Italian Istituto Nazionale di Fisica Nucleare; the Ministry of Education, Culture, Sports, Science and Technology of Japan; the Natural Sciences and Engineering Research Council of Canada; the National Science Council of the Republic of China; the Swiss National Science Foundation; the A.P. Sloan Foundation; the Bundesministerium für Bildung und Forschung, Germany; the Korean Science and Engineering Foundation and the Korean Research Foundation; the Science and Technology Facilities Council and the Royal Society, UK; the Institut National de Physique Nucleaire et Physique des Particules/CNRS; the Russian Foundation for Basic Research; the Ministerio de Ciencia e Innovación, and Programa Consolider-Ingenio 2010, Spain; the Slovak R&D Agency; and the Academy of Finland.

[1] P. W. Higgs, Phys. Lett. **12**, 132-133 (1964).
[2] M.Cacciari *et al.*, JHEP **04**, 68 (2004); N.Kidonakis and R. Vogt, Phys. Rev. D **68**, 114014 (2003).
[3] W.-M. Yao *et al.* (Particle Data Group), J. Phys. G **33**, 1 (2006) and 2007 partial update for the 2008 edition.
[4] T. Aaltonen *et al.*, *Measurement of the Top Quark Mass with Dilepton Events Selected Using Neuroevolution at CDF*, Fermilab-Pub-08-369-E. arXiv:0807.4652v1. Submitted to Phys. Rev. Lett. July 29, (2008).
[5] T. Aaltonen *et al.*, *The First Measurement of the Top Quark Mass at CDF II in the Lepton+Jets and Dilepton Channels Simultaneously*, Fermilab-Pub-08-415-E. Submitted to Phys. Rev. D September 29, (2008).
[6] A. Abulencia *et al.* (CDF Collaboration), Phys. Rev. D **73**, 112006 (2006).
[7] F. Abe *et al.*, Nucl. Instrum. Methods, A **271**, 387 (1988); D. Amidei *et al.*, Nucl. Instrum. Methods, A **350**, 73 (1994); F. Abe *et al.* (CDF Collaboration), Phys. Rev. D **52**, 4784 (1995); P. Azzi *et al.*, Nucl. Instrum. Methods, A **360**, 137 (1995); R. Blair *et al.*, The CDF Run II Detector Technical Design Report, Fermilab-Pub-96/390-E.
[8] C.S. Hill *et al.*, Nucl. Instrum. Methods, A **530**, 1 (2004).
[9] A. Sill *et al.*, Nucl. Instrum. Methods, A **447**, 1 (2000).
[10] A. Affolder *et al.*, Nucl. Instrum. Methods, A **453**, 84 (2000).
[11] T. Affolder *et al.*, Nucl. Instrum. Methods, A **526**, 249 (2004).
[12] G. Apollinari *et al.*, Nucl. Instrum. Methods, A **412**, 515 (1998).
[13] G. Ascoli *et al.*, Nucl. Instrum. Methods, A **268**, 33 (1988).
[14] L. Balka *et al.*, Nucl. Instrum. Methods, A **267**, 272 (1988).
[15] A. Artikov *et al.*, FNAL-PUB-07-023-E, June, 2007.
[16] S. Bertolucci *et al.*, Nucl. Instrum. Methods, A **267**, 301 (1988).
[17] Y. Seiya *et al.*, Nucl. Instrum. Methods, A **480**, 524 (2002).
[18] E. Thomson *et al.*, IEEE Trans. Nucl. Sci. **49**, 1063 (2002).
[19] F. Abe *et al.* (CDF Collaboration), Phys. Rev. Lett. **80**, 2779 (1998).
[20] F. Abe *et al.* (CDF Collaboration), Phys. Rev. D **45**, 1448 (1992).
[21] A. Abulencia *et al.*, Nucl. Instrum. Methods, A **566**, 375 (2006).
[22] D. Acosta *et al.* (CDF Collaboration), Phys. Rev. D **71**, 52003 (2005).
[23] T. Sjostrand *et al.*, PYTHIA 6.216, Comput. Phys. Commun. **135**, 238 (2001).
[24] H.L. Lai *et al.*, Eur. Phys. J. C **12**, 375 (2000).
[25] E. Gerchtein and M. Paulini, ECONF C0303241, TUMT005 (2003), arXiv:physics/0306031.
[26] C. Mills, Ph.D. thesis, University of California, Santa Barbara, Fermilab-Thesis-2007-49.
[27] M. Cacciari, S. Frixione, M.L. Mangano, P. Nason, G. Ridolfi, JHEP **0404**, 068 (2004).
[28] A. Abulencia *et al.* (CDF Collaboration), Phys. Rev. D **73**, 032003 (2006).
[29] M. Jezabek and J.H. Kuhn, Nucl. Phys. B **314**, 1 (1989).
[30] M.L. Mangano, M. Moretti, F. Piccinini, R. Pittau, and A.D. Polosa, ALPGEN 2.10, JHEP **0307**, 001 (2003).
[31] F. James, *MINUIT: Function Minimization and Error Analysis*,CERN Program Library, **D506**.
[32] A. Bhatti *et al.*, Nucl. Instrum. Methods, A **566**, 375 (2006).
[33] A. Heister *et al.* (ALEPH Collaboration), Phys. Lett., B **512**, 30 (2001); G. Abbiendi *et al.* (OPAL Collaboration), Eur. Phys. J., C **29**, 463 (2003).
[34] K. Abe *et al.* (SLD Collaboration), Phys. Rev. D **65**, 92006 (2002).
[35] T. Sjostrand, Comput. Phys. Commun. **82**, 74 (1994); G. Marchesini *et al.*, Comput. Phys. Commun. **67**, 465 (1992).
[36] Y. L. Dokshitzer, Sov. Phys. JETP **46**, 641 (1977).
[37] A.D. Martin, R.G. Roberts, W.J. Stirling, and R.S. Thorne, Eur. Phys. J. C **14**, 133 (2000); A.D. Martin *et al.*, Eur. Phys. J. C **39**, 155 (2005).
[38] The Tevatron Electroweak Working Group, arXiv:hep-ex/0808.1089.